Phys. Status Solidi B **247**, No. 7, 1740–1746 (2010) / **DOI** 10.1002/pssb.200983656

physica status solidi b
www.pss-b.com
basic solid state physics

$Al_{1-x}In_xN$/GaN bilayers: Structure, morphology, and optical properties

K. Lorenz[*,1,2], S. Magalhães[1,3], N. Franco[1,2], N. P. Barradas[1,2], V. Darakchieva[1,2], E. Alves[1,2], S. Pereira[3], M. R. Correia[3], F. Munnik[4], R. W. Martin[5], K. P. O'Donnell[5], and I. M. Watson[6]

[1] Instituto Tecnológico e Nuclear, Estrada Nacional 10, 2696-953 Sacavém, Portugal
[2] Centro de Física Nuclear da Universidade de Lisboa, Av. Prof. Gama Pinto 2, 1649-003 Lisboa, Portugal
[3] CICECO, Departamento de Física and I3N, Universidade de Aveiro, 3810-193 Aveiro, Portugal
[4] Forschungszentrum Dresden Rossendorf, 01314 Dresden, Germany
[5] Department of Physics, SUPA, University of Strathclyde, Glasgow G4 0NG, UK
[6] Institute of Photonics, SUPA, University of Strathclyde, Glasgow G4 0NW, UK

Received 9 November 2009, revised 7 January 2010, accepted 6 February 2010
Published online 3 June 2010

Keywords photoluminescence, Rutherford backscattering spectrometry, surface structure, III–V semiconductors

[*] Corresponding author: e-mail Lorenz@itn.pt, Phone: +351 21994 6052, Fax: +351 21994 6285

High quality $Al_{1-x}In_xN$/GaN bilayers, grown by metal organic chemical vapor deposition (MOCVD), were characterized using structural and optical techniques. Compositional analysis was performed using Rutherford backscattering spectrometry (RBS) and elastic recoil detection analysis (ERDA). The InN molar fraction x decreased approximately linearly with increasing growth temperature and ranged from $x=0.13$ to 0.24. Up to $x=0.20$ the layers grow pseudomorphically to GaN with good crystalline quality. These layers show a smooth surface with V-shaped pits. Two layers with InN contents around 24% showed partial strain relaxation. However, the mechanisms leading to relaxation of compressive strain are very different in the two samples grown both at similar temperature but with different growth rates. One sample shows a decreased c/a ratio, as expected for relaxation of the compressive strain, while In was shown to be homogeneously distributed with depth. The other sample started to grow with $x=0.24$ but relaxed mainly by reduction of the incorporated InN content towards the lattice-match composition of $x\sim0.17$. Both samples have an increased surface roughness. All samples show strong $Al_{1-x}In_xN$ band edge luminescence with large bowing parameter and Stokes' shifts.

© 2010 WILEY-VCH Verlag GmbH & Co. KGaA, Weinheim

1 Introduction $Al_{1-x}In_xN$ alloys cover the widest wavelength range among the III-nitride ternaries with band gaps at room temperature from ~0.6 eV (InN) to ~6.2 eV (AlN). Furthermore, $Al_{1-x}In_xN$ can be grown lattice-matched to GaN with an InN content around 17–18%, allowing the growth of heterostructures with negligible biaxial strain. Since the lattice-matched $Al_{0.82}In_{0.18}N$ shows both a higher band gap (~4.4 eV) than GaN and a much smaller refractive index, this material is well suited for inclusion in distributed Bragg reflectors and microcavities. A recent review article on these topics was provided by Butté et al. [1]. Also the potential of $Al_{1-x}In_xN$/GaN heterostructures for high electron mobility transistor structures is under investigation [2–4] as well as device processing techniques such as selective wet etching [5, 6] and ion implantation [7, 8]. Although the large immiscibility of AlN and InN renders $Al_{1-x}In_xN$ growth difficult [9–11], high quality thin films have been grown by metal organic chemical vapor deposition (MOCVD) [1–4, 11–14], MBE [15, 16], and reactive sputtering [17, 18], in particular close to the lattice-match composition. Nevertheless, the physical properties of the alloy remain controversial. The first issue is an accurate determination of alloy composition, which in turn affects the dependencies of the band gap and the strain. Recent experimental results on MOCVD and sputtered samples revealed discrepancies between the InN molar fractions measured by Rutherford backscattering spectrometry (RBS) and X-ray diffraction (XRD) [12, 17, 19]. The deviations are partly due to the breakdown of Vegard's law in the $Al_{1-x}In_xN$ system as also predicted theoretically [20]. This breakdown, together with inaccuracies in the values of elastic and lattice constants of the binaries, in particular InN, will lead to systematic errors when the film composition is extracted conventionally from XRD measurements.

WILEY InterScience® DISCOVER SOMETHING GREAT

© 2010 WILEY-VCH Verlag GmbH & Co. KGaA, Weinheim

Additionally, defects and impurities can introduce hydrostatic or uniaxial strain. RBS allows the *direct* measurement of the InN content independently of the strain state and the material parameters of the binaries InN and AlN but is insensitive to the presence of light elements. In combination with ion channeling, RBS/C (channeling) offers in addition the possibility to assess crystal quality and strain as a function of depth.

Elastic recoil detection analysis (ERDA), as a complement to RBS, is more sensitive to light elements, allowing the determination of the nitrogen stoichiometry and detection of low atomic number impurities.

In this review we describe structural, morphologic, and optical characterization of a set of $Al_{1-x}In_xN$/GaN samples with InN molar fractions ranging from $x = 0.13$ to 0.24, therefore changing from tensile to compressive strain with increasing x. $Al_{1-x}In_xN$ with an InN fraction up to 20% grows pseudomorphically to GaN with good structural and optical properties. The compressive strain relaxations of the two films with highest InN content show distinct differences.

2 Experimental details $Al_{1-x}In_xN$ films were grown on ~1 μm thick GaN buffer layers on (0001) sapphire substrates by MOCVD in an Aixtron 200 series reactor. The growth parameters for all samples are summarized in Table 1. The molar flow rates of the reactants trimethylaluminum (TMAl), trimethylindium (TMIn), and ammonia were kept constant at 22.0, 14.0, and 223 μmol/min, respectively, except for sample S800a which was grown with a slightly higher TMAl flow rate (Table 1); the InN molar fraction was controlled by changing the growth temperature from 760 to 840 °C. The sample set consists of two series; structural and optical characterization results of the first series (samples S760, S800, S820, and S840) have been published in Refs. [12, 21, 22]; the second series (samples S770 and S810) was grown under similar conditions. The growth rates were ~60 nm/h for sample series 1 and were approximately doubled for the second sample set due to intervening changes in the internal geometry of the reactor between growth runs.

RBS/C measurements were performed to assess crystalline quality, composition, and strain using 1.5 or 2 MeV He^+ ions and silicon surface barrier detectors at scattering angles of 140 or 160°. The random RBS spectra were taken by tilting the sample off the normal by 5° and rotating it during the measurement, in order to suppress channeling effects, and fitted using the NDF code [23]. Angular scans were performed with a two-axes goniometer controlled by stepping motors with an accuracy of 0.01°.

Heavy ion ERDA measurements were performed using a $^{35}Cl^{7+}$ 35 MeV beam. The recoils and scattered beam were detected in a Bragg ionization chamber and hydrogen was simultaneously measured using a surface barrier detector [24].

XRD reciprocal space map (RSM) and rocking curve (RC) characterizations were performed using monochromated Cu $K\alpha_1$ radiation on a D8 Discover system from Bruker-AXS using a Göbel mirror, an asymmetric 2-bounce Ge(220) monochromator and a scintillation detector. The RCs were acquired with an open detector without slits or analyzer in the secondary beam, while the RSMs were recorded with a 1 mm slit in front of the detector. Some RSM were taken in another high resolution system using a position sensitive detector.

Atomic force microscopy (AFM) measurements were performed in tapping mode with a commercial MultiMode scanning probe microscope (Nanoscope IIIA, DI).

Photoluminescence (PL) measurements were done by exciting samples at room temperature with 244 nm light from a frequency-doubled Ar ion laser or at 10–15 K with a monochromated Xe lamp [22].

3 Results and discussion Figure 1 plots the InN fractions measured by RBS and ERDA as a function of the growth temperature. An approximately linear correlation is found in the investigated composition range, similar to that in InGaN grown under comparable conditions and in good agreement with computational modeling of the InN incorporation during MOCVD growth [25, 26]. The InN incorporation in the two sample series is similar despite the large difference in growth rate. The InN composition can therefore be controlled most effectively by varying the growth temperature, although increasing the TMAl flow (sample S800a) has a small but noticeable effect. This observation is in good agreement with a recent detailed study

Table 1 Growth parameters (TMAl and TMIn flow rates, growth rates, and growth temperatures), thicknesses, RBS/C minimum yields χ_{min}, and XRD rocking curve FWHMs for the 0004 and $10\bar{1}4$ reflections.

sample	TMAl and TMIn flow rates (μmol/min)	growth rate (nm/h)	$Al_{1-x}In_xN$ growth temperature (°C)	thickness RBS (nm) (±10 nm)	χ_{min} (%) RBS (±0.5%)	XRD FWHM 0004 RC (arcsec)	XRD FWHM $10\bar{1}4$ RC (arcsec)
S760	22 and 14	60	760	126	≈40	n.a.	n.a.
S770	22 and 14	143	770	143	30	n.a.	n.a.
S800	22 and 14	63	800	126	6.3	552	572
S800a	29.5 and 14	61.5	800	123	7.0	669	693
S810	22 and 14	124	810	124	3.0	446	478
S820	22 and 14	64	820	128	4.0	463	491
S840	22 and 14	61	840	122	4.4	447	490

© 2010 WILEY-VCH Verlag GmbH & Co. KGaA, Weinheim

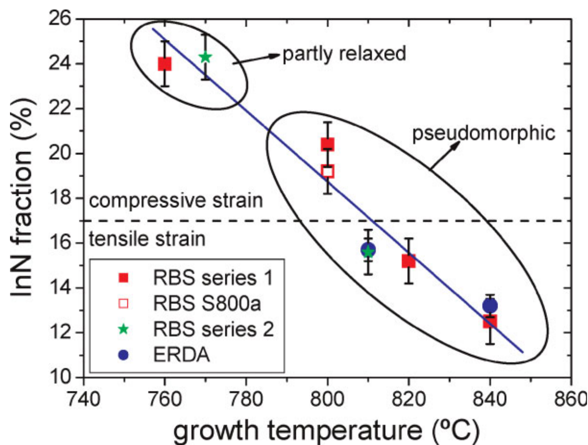

Figure 1 (online color at: www.pss-b.com) The InN molar fraction measured by RBS *versus* the growth temperature. The composition of two samples was also measured by heavy ion ERDA. The horizontal line marks the lattice-matched composition according to Vegard's law. Note that this position, which also depends on the *a* lattice constant of the GaN buffer layer, may be affected by deviations from Vegard's law, inaccuracy of the lattice parameters of the binaries AlN and InN and by the presence of hydrostatic or uniaxial strain.

on indium incorporation dynamics in $Al_{1-x}In_xN$ grown with TMIn fluxes exceeding that of TMAl [13].

Figure 2 presents RBS/C random and aligned spectra for three selected samples. All samples show a homogeneous depth distribution of In except layer S760 for which a compositional gradient is observed with InN content decreasing towards the surface. The displayed fit assumed a layer ~60 nm thick with $x = 0.24$ above the AlInN/GaN interface, followed by a second layer, of equal thickness, with a lower InN content of $x \sim 0.19$.

In the RBS spectra of Fig. 2 the signal due to lighter elements is superimposed on that of Ga in the GaN buffer. While the signal due to Al is well resolved it is not possible to distinguish the signal from nitrogen and light impurities. To analyze the RBS data it was assumed that the films have a stoichiometric nitrogen content of 50% and that the contamination by light impurities is negligible. In order to test these assumptions heavy ion ERDA measurements were performed on two samples.

During the ERDA measurements, light atom recoils and Cl-ions scattered at In and Ga atoms are detected in a Bragg ionization chamber which is sensitive to the atomic number Z as well as the total energy of the detected particles.

A typical ERDA map is shown in Fig. 3 in which each branch corresponds to one recoiled element. From each branch a spectrum is extracted which allows the determination of the elemental depth profile. The nitrogen stoichiometry of the layers was confirmed and composition measurements agree well with the RBS results (see Fig. 1). The ERDA map in Fig. 3 shows, in addition to the main constituents In, Al, and N, some surface contamination with carbon and oxygen.

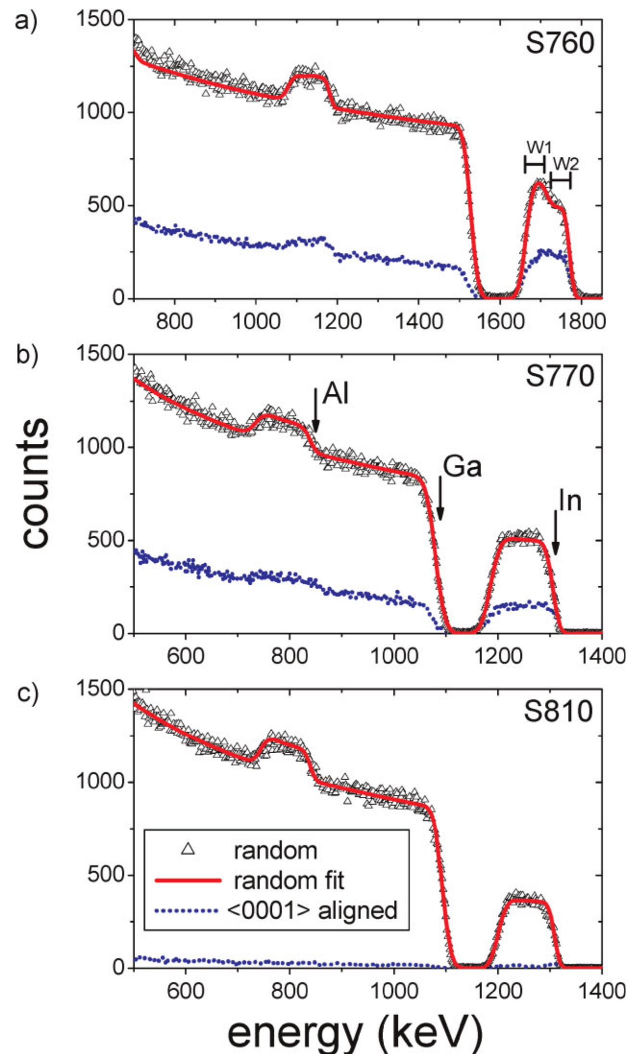

Figure 2 (online color at: www.pss-b.com) RBS/C random and ⟨0001⟩ aligned spectra of samples S760, S770, and S810. Note that the spectra of sample S760 were taken with a 2 MeV He^+ beam while the other two samples were measured with 1.5 MeV.

Additionally, large amounts of hydrogen are found, but due to the limited depth resolution of the H detection set-up and the small film thickness it is not possible to discriminate between a strong contamination of a thin surface layer, typical for nitride semiconductors [27, 28], and hydrogen in the bulk of the layer.

Table 1 provides two measures of crystal quality, namely values of the RBS/C minimum yield χ_{min} (backscattering yield of the aligned RBS/C spectrum divided by the random yield) for a window on the In-signal and also XRD RC full widths at half maximum (FWHMs) for the symmetric 0004 and the asymmetric $10\bar{1}4$ reflections. The In minimum yield is increased by interstitial In as well as by defects that cause a displacement of In perpendicular to the *c*-axis; for comparison, a typical value of χ_{min} for state-of-the-art GaN films is ~2%. The RC FWHM of a thin film depends on the layer thickness and is further broadened by structural

© 2010 WILEY-VCH Verlag GmbH & Co. KGaA, Weinheim

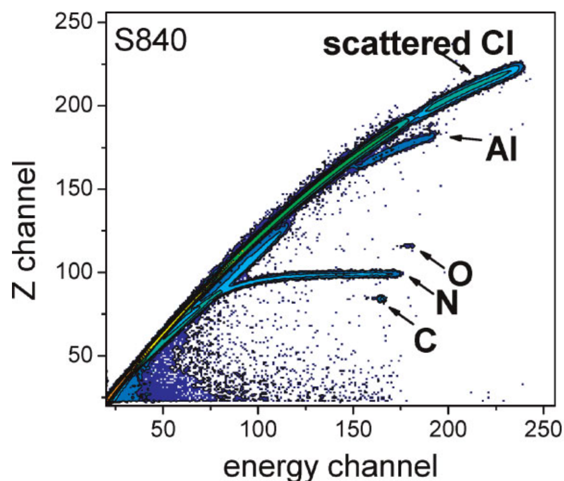

Figure 3 (online color at: www.pss-b.com) Heavy ion ERDA map of sample S840 showing the signal of recoiled light elements and the Cl beam scattered from In and Ga. Besides the main constituents In, Al, and N some surface contamination by C and O is also revealed.

imperfections such as dislocations, inhomogeneous strain, and compositional fluctuations. Since the layers discussed here have similar thicknesses their FWHM can be directly compared with each other: broader RCs indicate lower crystalline quality.

A good agreement between the two measures of quality (RBS/C minimum yield and RC FWHMs) is found, both indicating a deterioration of quality with increasing InN content. Note that XRD analysis of $Al_{1-x}In_xN$/GaN with similar lattice parameters of film and buffer layer is often not possible due to the overlap of the reflections from $Al_{1-x}In_xN$ and GaN. In these cases (marked not applicable, n.a., in Table 1) RBS/C proves particularly useful to measure composition, quality, and strain.

A high minimum yield is seen in Fig. 2 for the two samples (S760 and S770) grown at the lowest temperatures. Furthermore, for sample S760 the layer close to the GaN interface shows a better RBS/C minimum yield but a strong deterioration of crystal quality accompanies the compositional grading towards the surface (see also Ref. [21]).

XRD RSM around the $10\bar{1}5$ reciprocal lattice points for the entire composition region are presented in Fig. 4. For most samples the reflections for $Al_{1-x}In_xN$ and GaN lie on a vertical line confirming the pseudomorphic growth of these layers. For sample S760 only the signal from the $Al_{0.81}In_{0.19}N$ layer close to the surface is visible since the signal of the near-interface region with $x = 0.24$ is masked by the intense GaN peak [21]. The position of this peak is slightly shifted from the pseudomorphic position [21]. The RSM furthermore shows a high level of diffuse scattering due to the large number of defects present in this layer.

By performing full angular RBS/C scans across a tilted crystal axis within the plane containing both the *c*-axis and the tilted axis, it is possible to assess strain in pseudomorphic films and study strain relaxations with depth resolution. Strain relaxation causes a change of the *c/a* (*c* and *a* lattice parameters) ratio and therefore alters the angle Φ between the *c*-axis and the tilted axis. For the $\langle\bar{2}113\rangle$ axis in wurtzite nitrides the relation $\tan\Phi = a/c$ holds [12].

Figure 5 presents angular scans across the $\langle\bar{2}113\rangle$ axis of the three films shown in Fig. 2. Two energy windows were selected corresponding to In in the region near the interface with GaN (W1) and the surface region (W2). The two windows were exemplified in the RBS/C spectra of sample S760 in Fig. 2a. A shift between the scans of the two windows is related to a strain relaxation with depth as clearly observed for samples S760 and S770 while no such shift is visible for sample S810.

The exact determination of the degree of strain relaxation is made complicated by ion steering effects in the interface, which are difficult to quantify in non-perfect crystals [29]. Nevertheless, qualitative observations are very insightful in this case. Both films (S760 and S770) show a better quality close to the interface (better minimum yield for window W1) and crystal quality is deteriorating with increasing film thickness as expected for relaxation.

However, the mechanism for relaxation is different in the two films. Strain in layer S760 is mainly reduced by the decrease of the InN fraction towards the lattice-matched value, from 24% at the interface to 19% at the surface. The *a* lattice constant in this case changes only slightly from the pseudomorphic situation [21]. In contrast, layer S770 has a

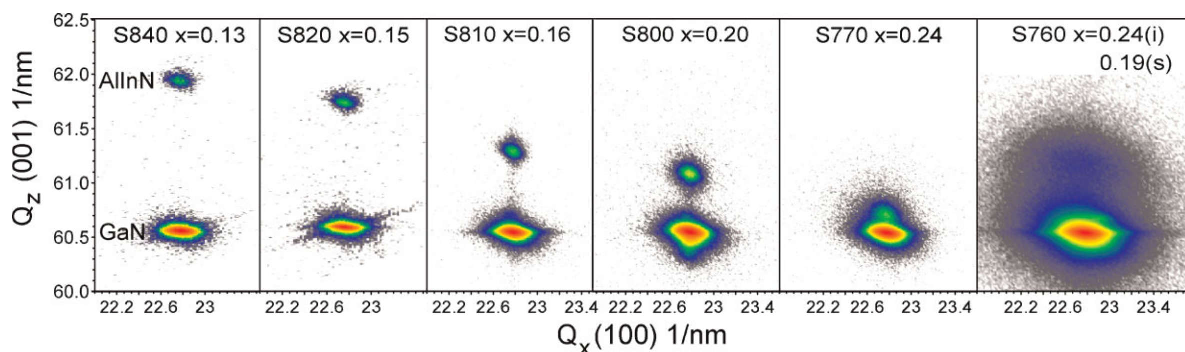

Figure 4 (online color at: www.pss-b.com) XRD RSM around the $10\bar{1}5$ reflection for samples in the composition range from $x = 0.13$ to 0.24.

© 2010 WILEY-VCH Verlag GmbH & Co. KGaA, Weinheim

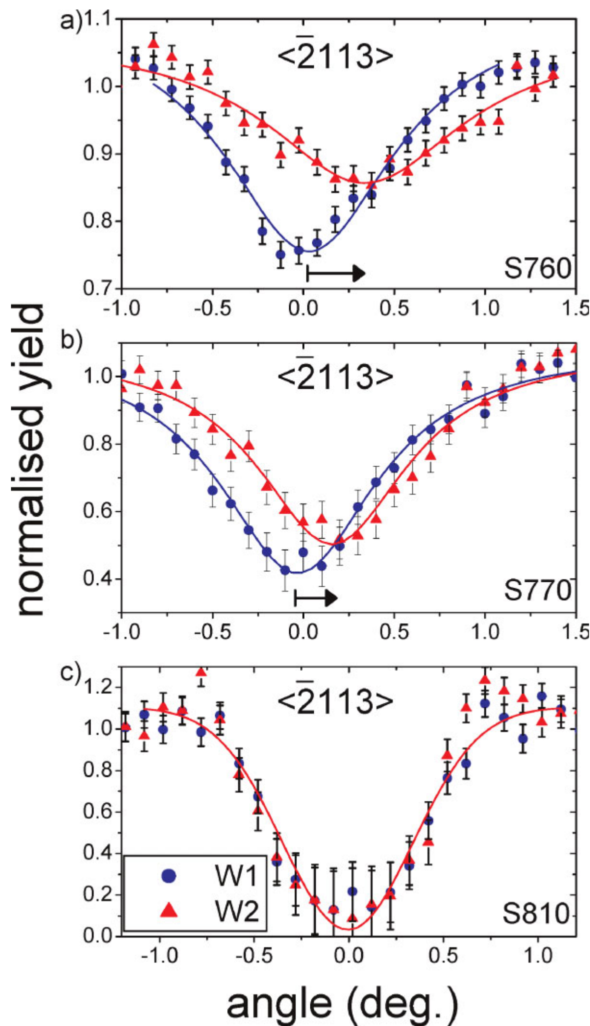

Figure 5 (online color at: www.pss-b.com) Angular RBS/C scans across the $\langle\bar{2}113\rangle$ axes of samples S760, S770, and S810 using two different energy windows on the In signal as indicated in Fig. 2a, corresponding to the region near the AlInN/GaN interface (W1) and the surface (W2).

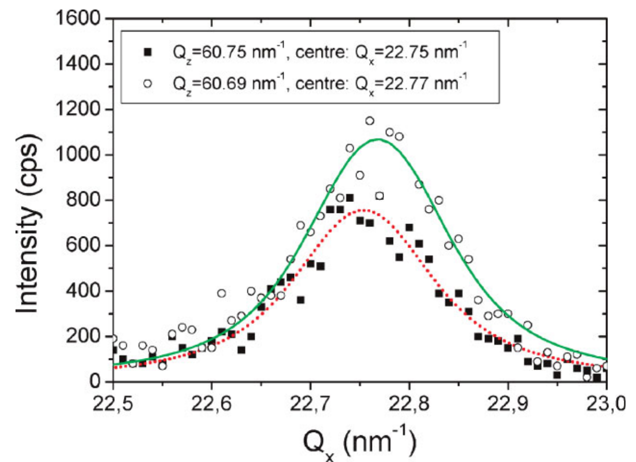

Figure 6 (online color at: www.pss-b.com) Horizontal cuts through the $10\bar{1}5$ RSM of sample S770. The relative shift of the curves confirms the partial relaxation of the layer towards the surface.

homogeneous In distribution throughout the film thickness and strain relaxation proceeds by the increase (decrease) of the a (c) lattice parameter. The RSM for sample S770 (Fig. 4) also shows some degree of relaxation confirming the RBS/C results. The gradual relaxation of the layer is better seen in horizontal cuts through the $Al_{1-x}In_xN$ reflection in the RSM (Fig. 6) which show an increase of the a lattice parameter for the cut corresponding to a lower c lattice parameter as expected for the relaxation of compressive strain.

The decrease of crystal quality in the partly relaxed samples is also reflected in their morphology. Figure 7 presents AFM images of samples S760, S770, and S810. Pseudomorphic films like S810 feature relatively smooth surfaces (root mean square (rms) roughness of ~0.6 nm) with hillocks of diameter ~100 nm and deep V-shaped pits that are typical for (0001) grown III-nitride films [30]. For sample S770, the rms roughness is slightly larger (~2 nm) and the morphology looks quite different: no pits are visible, suggesting that when the film starts to relax the pits are overgrown and a three-dimensional growth mode sets in, which results in the changed morphology. For sample S760 the rms roughness is significantly higher (~6 nm) and three-dimensional island growth is observed.

The reasons for the pronounced differences in relaxation mechanisms of samples S760 and S770 are so far not clearly understood. Both the small difference in growth temperature and the difference in growth rate may influence the relaxation mechanisms.

Photoluminescence spectra of all the samples in this study showed a strong composition-dependent $Al_{1-x}In_xN$ band edge emission superimposed upon the PL peak related to the under-lying GaN. The position of the $Al_{1-x}In_xN$ peak shifts to lower energies with increasing InN content. Figure 8 presents the PL peak energy *versus* the InN fraction measured by RBS. The inset of Fig. 8 shows typical PL spectra for two films with different composition upon laser excitation at room temperature. PL excitation measurements [22] at the peak of the $Al_{1-x}In_xN$ PL measure the alloy band-gap, revealing a very large bowing parameter (>6 eV) and Stokes' shifts much larger than those found for the related semiconductor InGaN [31]. Large and composition-dependent bowing parameters in AlInN and InGaN are also reported in a recent theoretical study which furthermore shows that clustering of In affects the band gap significantly and may be the cause of the large observed Stokes' shifts [32].

4 Summary A set of high quality $Al_{1-x}In_xN$/GaN bilayers was characterized using structural and optical techniques. The InN molar fraction x was controlled by changing the growth temperature and ranged from $x = 0.13$ to 0.24. Up to $x = 0.20$ the layers grow with good crystalline quality and pseudomorphically to GaN. These layers show a smooth surface with V-shaped pits. Two layers with InN

© 2010 WILEY-VCH Verlag GmbH & Co. KGaA, Weinheim

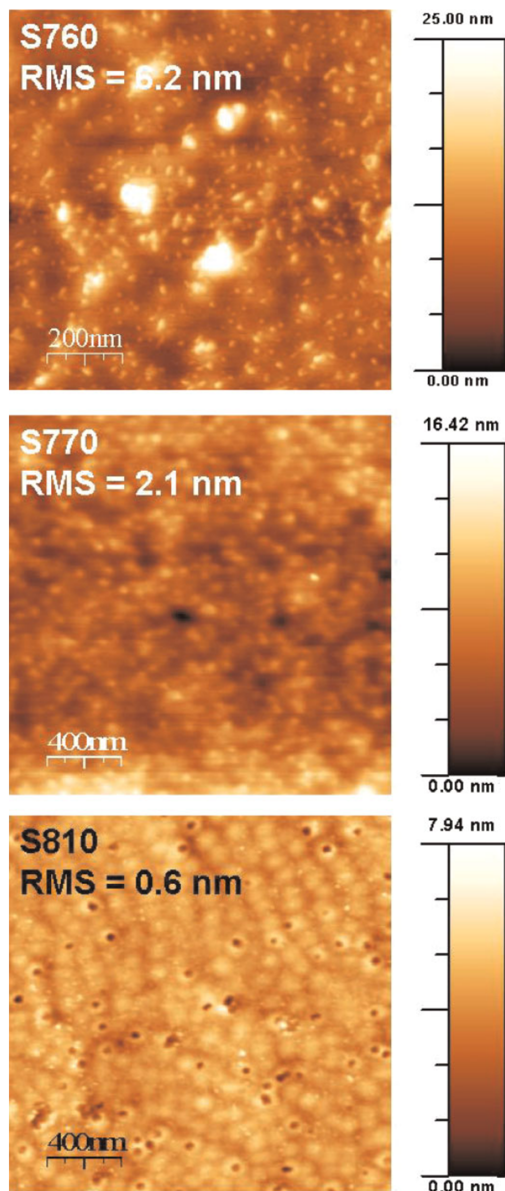

Figure 7 (online color at: www.pss-b.com) AFM images of samples S760, S770, and S810. Sample S810 shows the typical morphology of pseudomorphic layers with hillocks of diameter ~100 nm and V-shaped pits. The partially relaxed sample S770 shows a roughening of the surface and sample S760 exhibits a three-dimensional island growth.

content around 24% showed partial strain relaxation. However, the mechanisms leading to relaxation of compressive strain are very different in the two samples grown at similar temperature but with different growth rates. One sample shows a decrease of the *c/a* ratio as expected for the relaxation of compressive strain while In was found to be homogeneously distributed with depth. The other sample started to grow with $x = 0.24$ but relaxed mainly by reducing the incorporated InN content towards the lattice-match

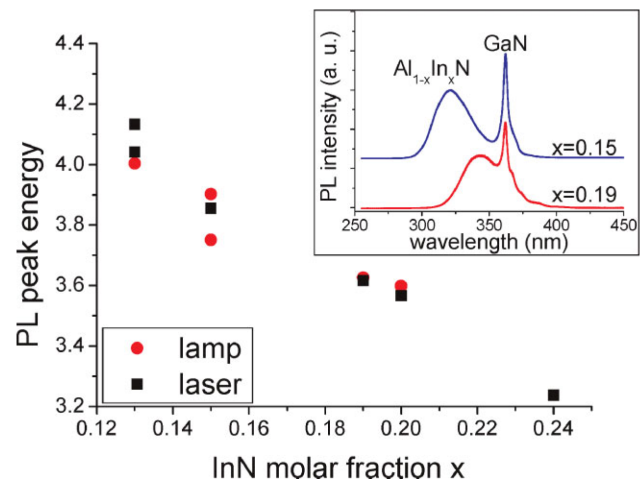

Figure 8 (online color at: www.pss-b.com) PL peak energy *versus* InN molar fraction measured by RBS. Squares and circles denote the results for RT laser and 15 K lamp excitations, respectively. Sample S820 ($x = 0.15$) reveals a double peak structure for lamp excitation and sample S840 ($x = 0.13$) shows some lateral changes of emission energy possibly due to compositional changes.

composition. Both samples show an increased surface roughness, tending towards three-dimensional growth.

Preliminary ERDA measurements confirmed the RBS composition measurements and the nitrogen stoichiometry of the films. Furthermore, some contamination with carbon, oxygen, and hydrogen was observed mainly at the surface.

Optical characterization reveals strong luminescence from the $Al_{1-x}In_xN$ with large bowing parameters and Stokes' shifts.

Acknowledgements We acknowledge funding by FCT Portugal (PTDC/FIS/65233/2006, BD/44635/2008, and "Ciência 2007"). The ERDA work was supported by the EU-"Research Infrastructures Transnational Access" program AIM "Center for Application of Ion Beams in Materials Research" under EC contract no. 025646.

References

[1] R. Butté, J.-F. Carlin, E. Feltin, M. Gonschorek, S. Nicolay, G. Christmann, D. Simeonov, A. Castiglia, J. Dorsaz, H. J. Buehlmann, S. Christopoulos, G. Baldassarri, H. von Högersthal, A. J. D. Grundy, M. Mosca, C. Pinquier, M. A. Py, F. Demangeot, J. Frandon, P. G. Lagoudakis, J. J. Baumberg, and N. Grandjean, J. Phys. D, Appl. Phys. **40**, 6328 (2007).

[2] A. Dadgar, F. Schulze, J. Bläsing, A. Diez, A. Krost, M. Neuburger, E. Kohn, I. Daumiller, and M. Kunze, Appl. Phys. Lett. **85**, 5400 (2004).

[3] O. Katz, D. Mistele, B. Meyler, G. Bahir, and J. Salzman, IEEE Trans. Electron. Devices **52**, 146 (2005).

[4] M. Gonschorek, J.-F. Carlin, E. Feltin, M. A. Py, and N. Grandjean, Appl. Phys. Lett. **89**, 062106 (2006).

[5] I. M. Watson, C. Xiong, E. Gu, M. D. Dawson, F. Rizzi, K. Bejtka, P. R. Edwards, and R. W. Martin, Proc. SPIE **6993**, 69930E (2008).

© 2010 WILEY-VCH Verlag GmbH & Co. KGaA, Weinheim

[6] D. Simeonov, E. Feltin, A. Altoukhov, A. Castiglia, J.-F. Carlin, R. Butté, and N. Grandjean, Appl. Phys. Lett. **92**, 171102 (2008).
[7] K. Lorenz, E. Alves, I. S. Roqan, R. W. Martin, C. Trager-Cowan, K. P. O'Donnell, and I. M. Watson, Phys. Status Solidi A **205**, 34 (2008).
[8] K. Wang, R. W. Martin, E. Nogales, P. R. Edwards, K. P. O'Donnell, K. Lorenz, E. Alves, and I. M. Watson, Appl. Phys. Lett. **89**, 131912 (2006).
[9] T. Matsuoka, Appl. Phys. Lett. **71**, 105 (1997).
[10] M. Ferhat and F. Bechstedt, Phys. Rev. B **65**, 075213 (2002).
[11] C. Hums, J. Bläsing, A. Dadgar, A. Diez, T. Hempel, J. Christen, A. Krost, K. Lorenz, and E. Alves, Appl. Phys. Lett. **90**, 022105 (2007).
[12] K. Lorenz, N. Franco, E. Alves, I. M. Watson, R. W. Martin, and K. P. O'Donnell, Phys. Rev. Lett. **97**, 85501 (2006).
[13] H. P. D. Schenk, M. Nemoz, M. Korytov, P. Vennéguès, A. D. Dräger, and A. Hangleiter, Appl. Phys. Lett. **93**, 081116 (2008).
[14] T. C. Sadler, M. J. Kappers, and R. A. Oliver, J. Cryst. Growth **311**, 3380 (2009).
[15] S. Fernández-Garrido, Ž. Gačević, and E. Calleja, Appl. Phys. Lett. **93**, 191907 (2008).
[16] E. Iliopoulos, A. Adikimenakis, C. Giesen, M. Heuken, and A. Georgakilas, Appl. Phys. Lett. **92**, 191907 (2008).
[17] T. Seppänen, L. Hultman, J. Birch, M. Beckers, and U. Kreissig, J. Appl. Phys. **101**, 043519 (2007).
[18] W. Terashima, S. B. Che, Y. Ishitani, and A. Yoshikawa, Jpn. J. Appl. Phys. **45**, L539 (2006).
[19] V. Darakchieva, M. Beckers, M.-Y. Xie, L. Hultman, B. Monemar, J.-F. Carlin, E. Feltin, M. Gonschorek, and N. Grandjean, J. Appl. Phys. **103**, 103513 (2008).
[20] V. Darakchieva, M.-Y. Xie, F. Tasnádi, I. A. Abrikosov, L. Hultman, B. Monemar, J. Kamimura, and K. Kishino, Appl. Phys. Lett. **93**, 261908 (2008).
[21] K. Lorenz, N. Franco, E. Alves, S. Pereira, I. M. Watson, R. W. Martin, and K. P. O'Donnell, J. Cryst. Growth **310**, 4058 (2008).
[22] K. Wang, R. W. Martin, D. Amabile, P. R. Edwards, S. Hernandez, E. Nogales, K. P. O'Donnell, K. Lorenz, E. Alves, V. Matias, A. Vantomme, D. Wolverson, and I. M. Watson, J. Appl. Phys. **103**, 073510 (2008).
[23] N. P. Barradas, C. Jeynes, and R. P. Webb, Appl. Phys. Lett. **71**, 291 (1997).
[24] U. Kreissig, S. Grigull, K. Lange, P. Nitzsche, and B. Schmidt, Nucl. Instrum. Methods B **136**, 674 (1998).
[25] E. V. Yakovlev, R. A. Talalaev, R. W. Martin, C. Jeynes, N. Peng, C. J. Deatcher, and I. M. Watson, Phys. Status Solidi C **3**, 1620 (2006).
[26] E. V. Yakovlev, A. V. Lobanova, R. A. Talalaev, I. M. Watson, K. Lorenz, and E. Alves, Phys. Status Solidi C **5**, 1688 (2008).
[27] V. Darakchieva, N. P. Barradas, M.-Y. Xie, K. Lorenz, E. Alves, M. Schubert, P. O. A. Persson, F. Giuliani, F. Munnik, C. L. Hsiao, L. W. Tu, and W. J. Schaff, Physica B **404**, 4476 (2009).
[28] F. G.-P. Flores, A. Redondo-Cubero, R. Gago, A. Bengoechea, A. Jiménez, D. Grambole, A. F. Braña, and E. Muñoz, J. Phys. D, Appl. Phys. **42**, 055406 (2009).
[29] A. Redondo-Cubero, K. Lorenz, R. Gago, N. Franco, S. Fernández-Garrido, P. J. M. Smulders, E. Muñoz, E. Calleja, I. M. Watson, and E. Alves, Appl. Phys. Lett. **95**, 051921 (2009).
[30] Th. Kehagias, G. P. Dimitrakopulos, J. Kioseoglou, H. Kirmse, C. Giesen, M. Heuken, A. Georgakilas, W. Neumann, Th. Karakostas, and Ph. Komninou, Appl. Phys. Lett. **95**, 071905 (2009).
[31] R. W. Martin, P. G. Middleton, K. P. O'Donnell, and W. van der Stricht, Appl. Phys. Lett. **74**, 263 (1999).
[32] I. Gorczyca, S. P. Łepkowski, T. Suski, N. E. Christensen, and A. Svane, Phys. Rev. B **80**, 075202 (2009).

© 2010 WILEY-VCH Verlag GmbH & Co. KGaA, Weinheim